

Observables predicted by HF theory

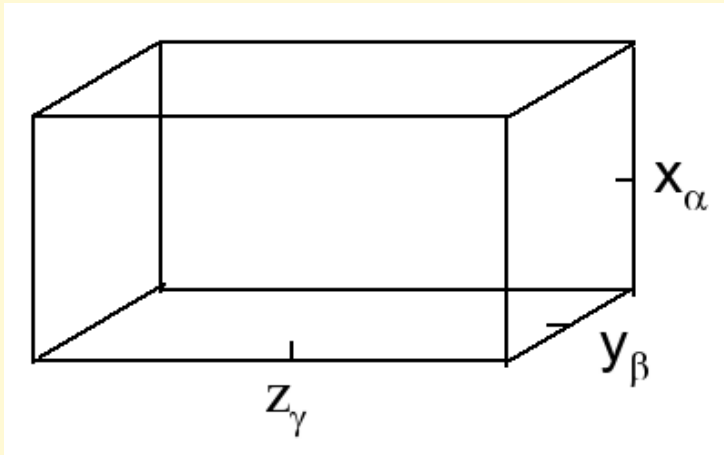
- Total **binding energy** of the nucleus in its ground state
⇒ separation energies for p / n (= BE differences)
- Ground state **density distribution of protons and neutrons**
⇒ mean square radii
⇒ EM multipole moments (for deformed g.s. density)
- **single particle levels** (energies, angular momenta, parity)
⇒ shell gaps (explains magic numbers)
⇒ Fermi levels for p / n

NOTE: HF is a **ground state** theory.

For **excited states** we need **Random Phase Approximation = RPA**

Static Hartree-Fock: numerical implementation

Represent wave functions for all A nucleons on 3-D Cartesian lattice



Grid points:

$$x_{\alpha} \quad (\alpha = 1, \dots, N_x)$$

$$y_{\beta} \quad (\beta = 1, \dots, N_y)$$

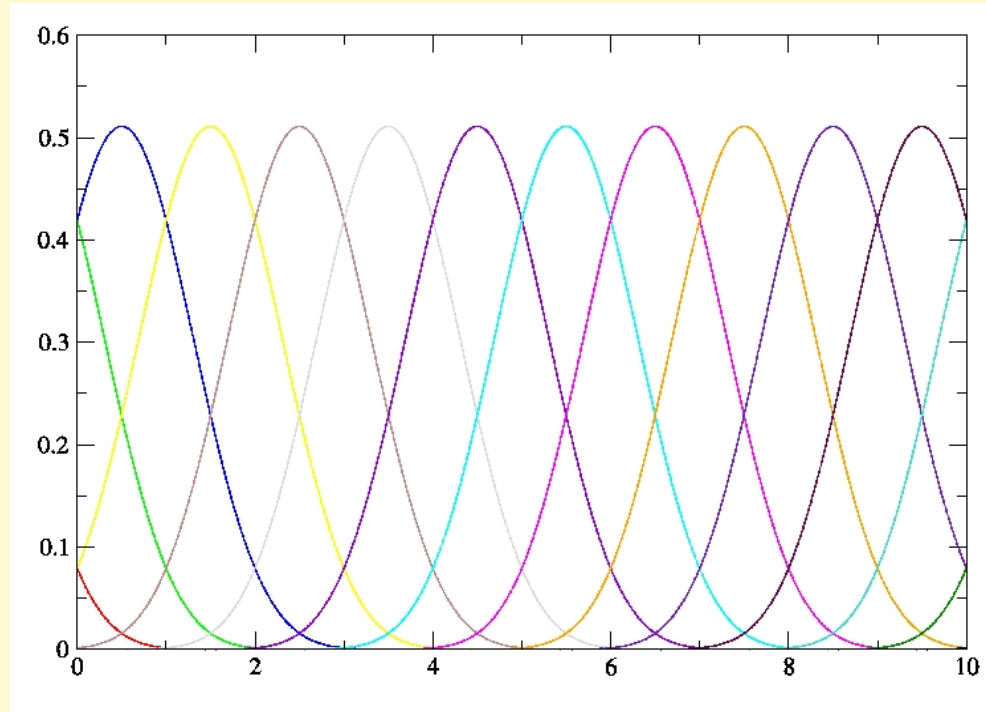
$$z_{\gamma} \quad (\gamma = 1, \dots, N_z)$$

$$\psi(x, y, z; \sigma_z, t_z) \rightarrow \psi(x_{\alpha}, y_{\beta}, z_{\gamma}; \sigma_z, t_z)$$

Wave function on the lattice becomes a complex-numbered array of dimension

$$\psi(N_x, N_y, N_z, 2, 2)$$

Basis-Splines (7th order), periodic boundary condition

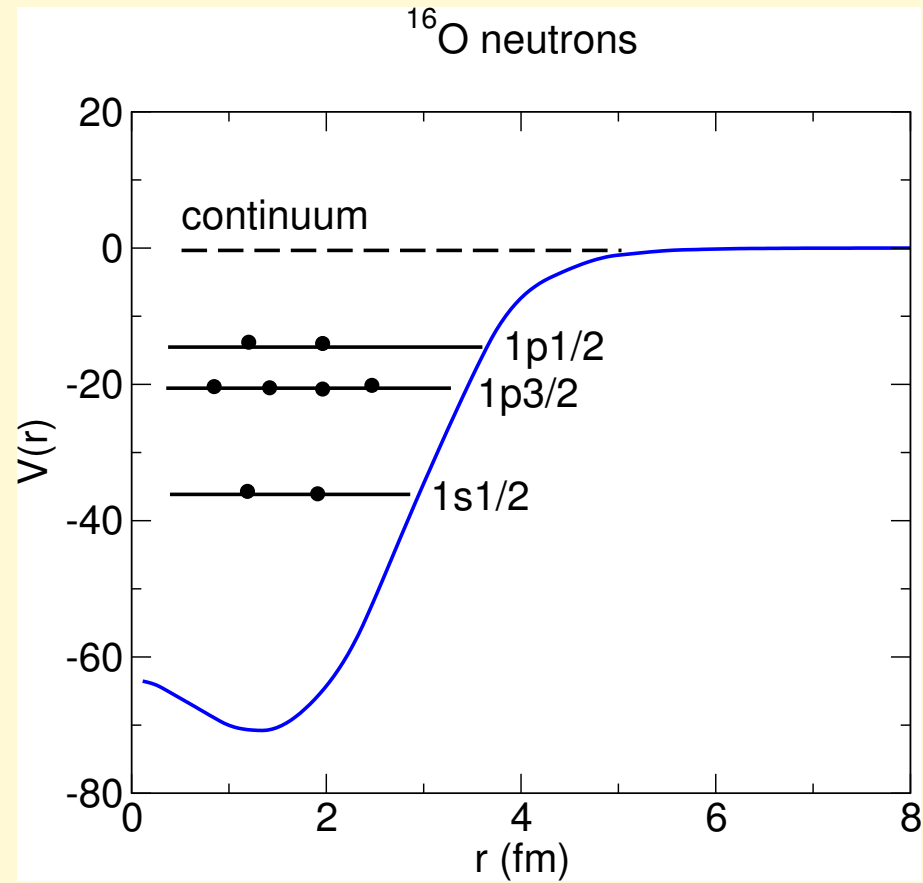
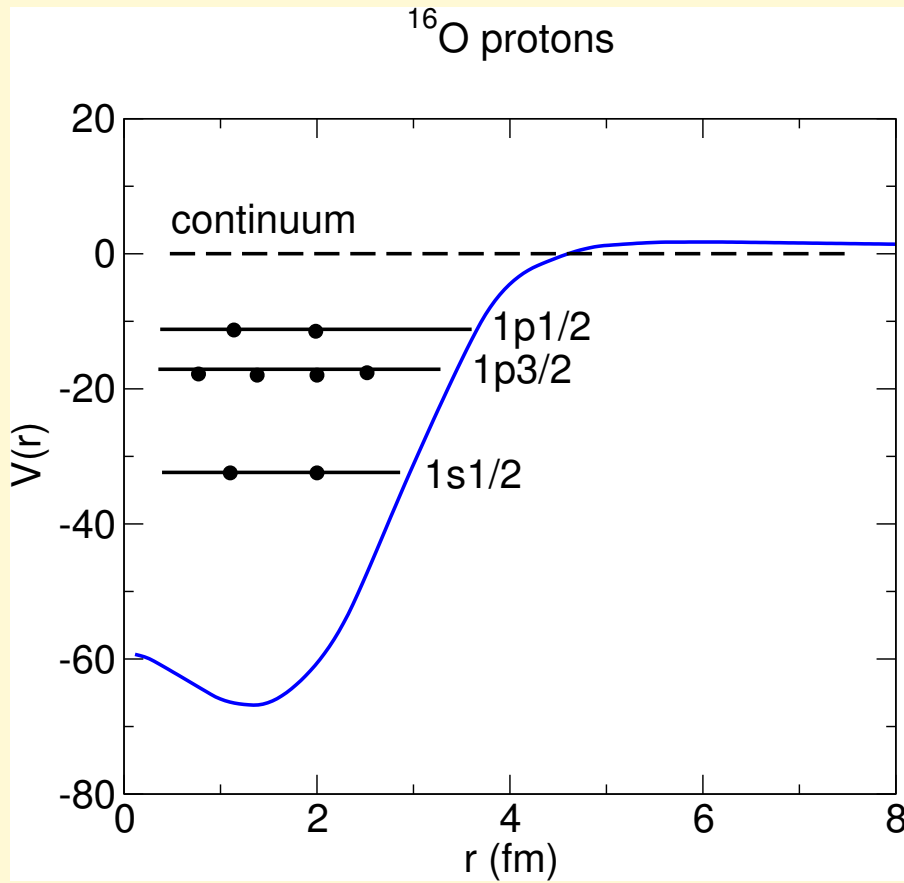


Expand wave function in terms of products of Basis-Spline functions

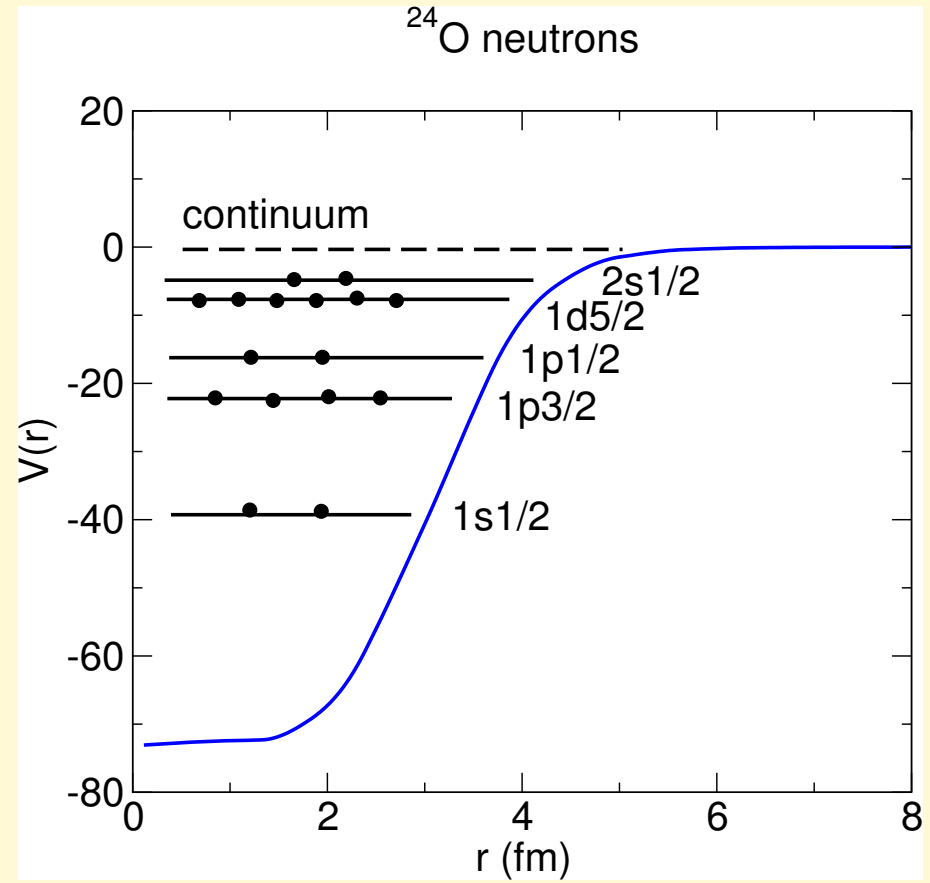
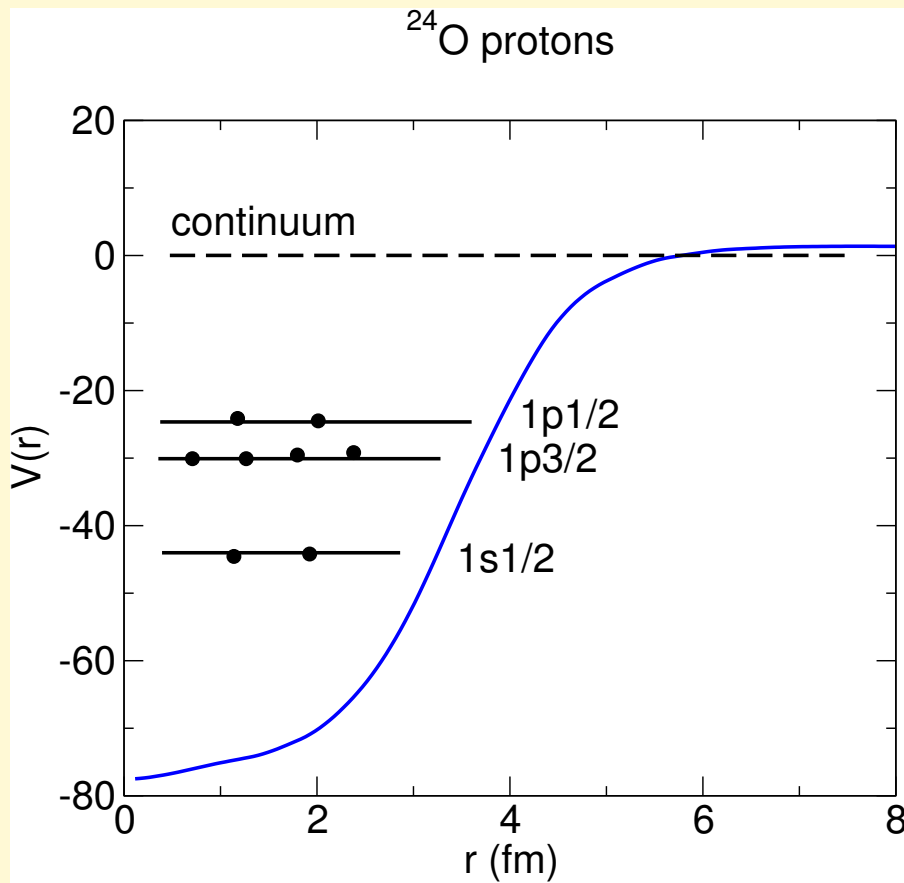
$$\psi(x, y, z; t) = \sum_{i,j,k} B_i(x) B_j(y) B_k(z) c^{ijk}(t)$$

Stable nucleus ^{16}O

HFB-2D calculation, SLy4 N-N interaction

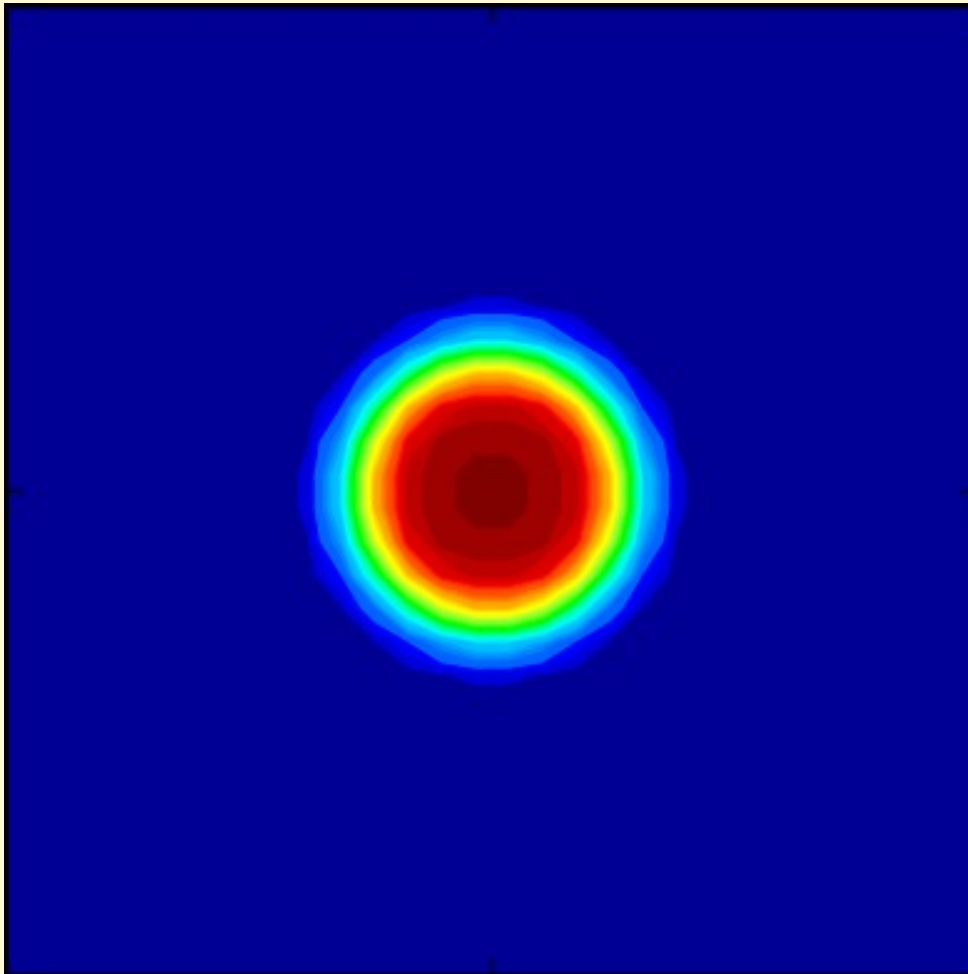


Neutron dripline nucleus ^{24}O ($T_{1/2} = 65$ ms)
HFB-2D calculation, SLy4 N-N interaction



^{48}Ca : HF predicts spherical density distribution,
in agreement with exp. data

620 static iterations, CPU time = 2m 21s (16 INTEL Xeon CPUs)



Convergence of total binding
energy $\Delta E / E = -5.7 \times 10^{-9}$

HF binding energy
= -431.10 MeV
exp. binding energy
= -416.00 MeV

accuracy = 3.4%

Charge densities for various nuclei (electron scattering data vs. theory)

Ref: J.W. Negele, Rev. Mod. Phys. 54, 913 (1982)

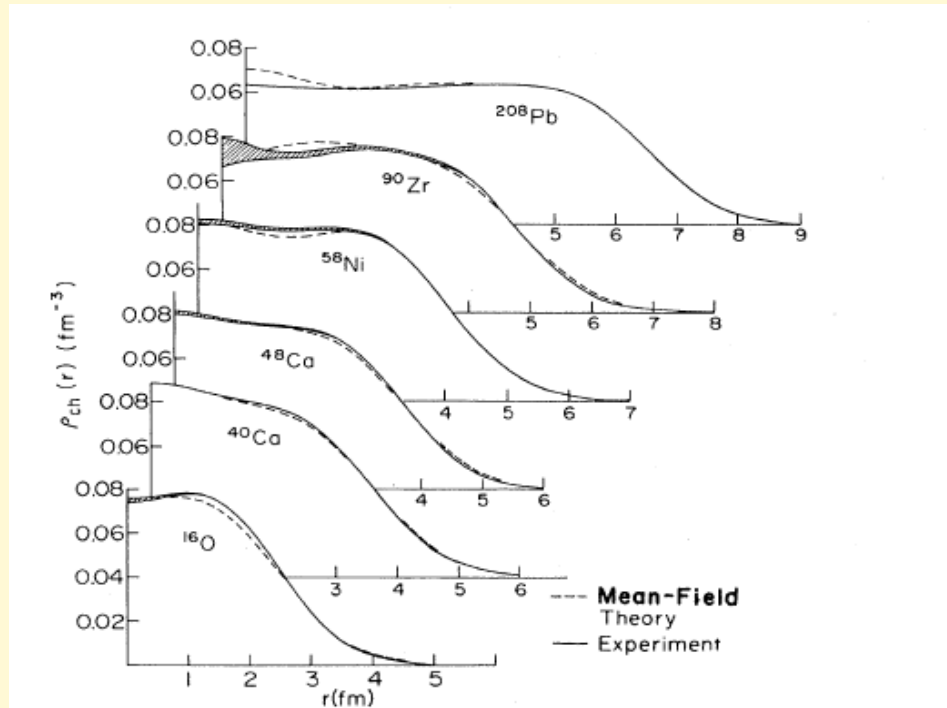
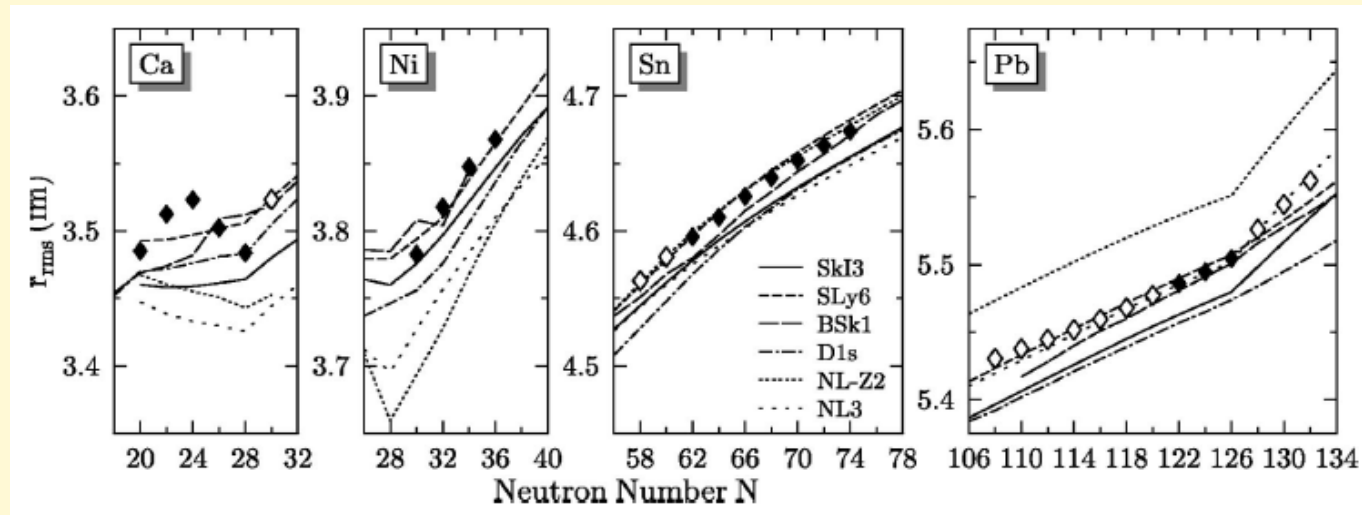


FIG. 11. Comparison of DME mean-field theory charge distributions in spherical nuclei (dashed lines) with empirical charge densities. The solid curves and shaded regions represent the error envelope of densities consistent with the measured cross sections and their experimental uncertainties.

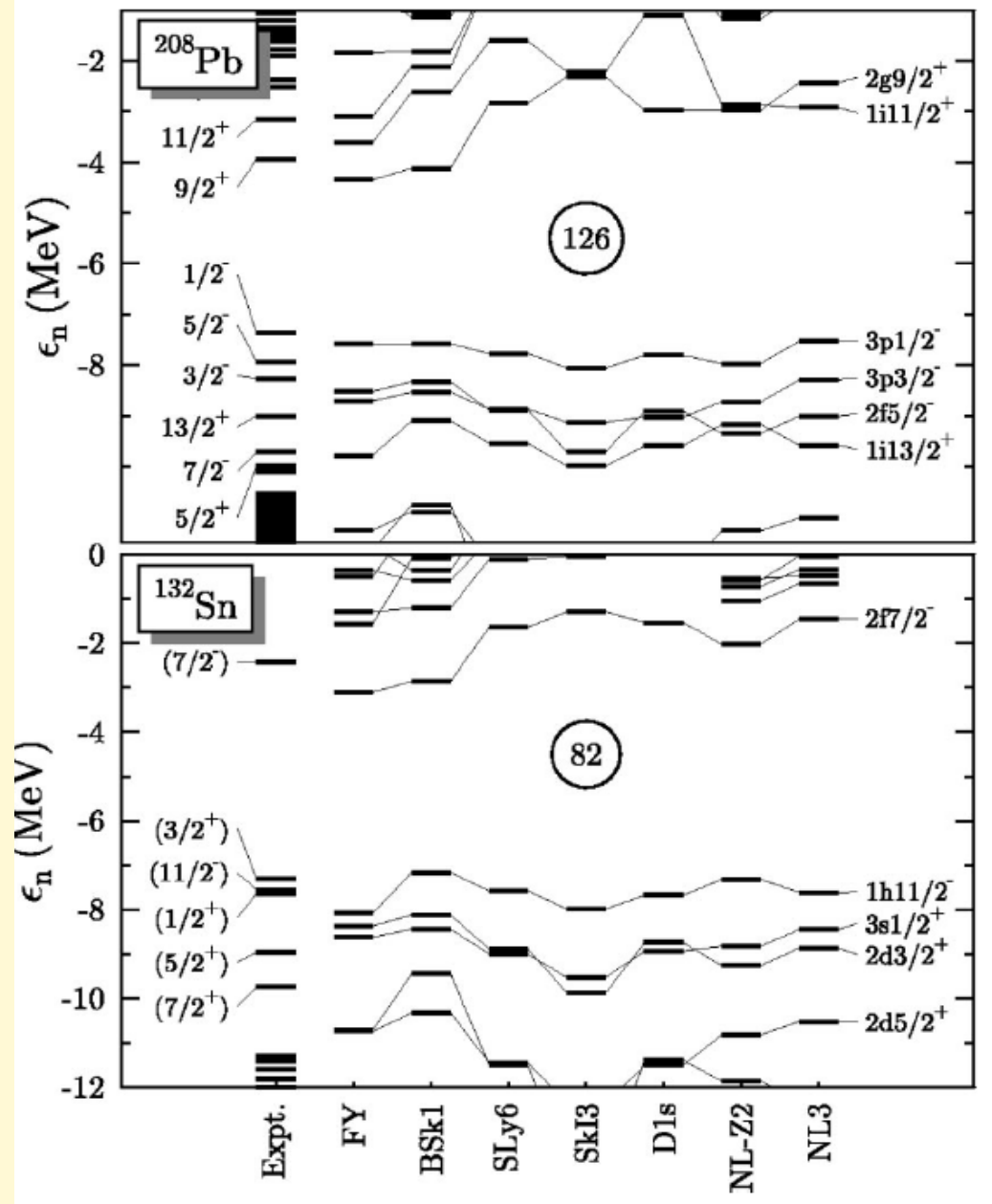
rms charge radii for several isotope chains.
HF calculation with different Skyrme forces, compared
to exp. data (filled and open diamonds)



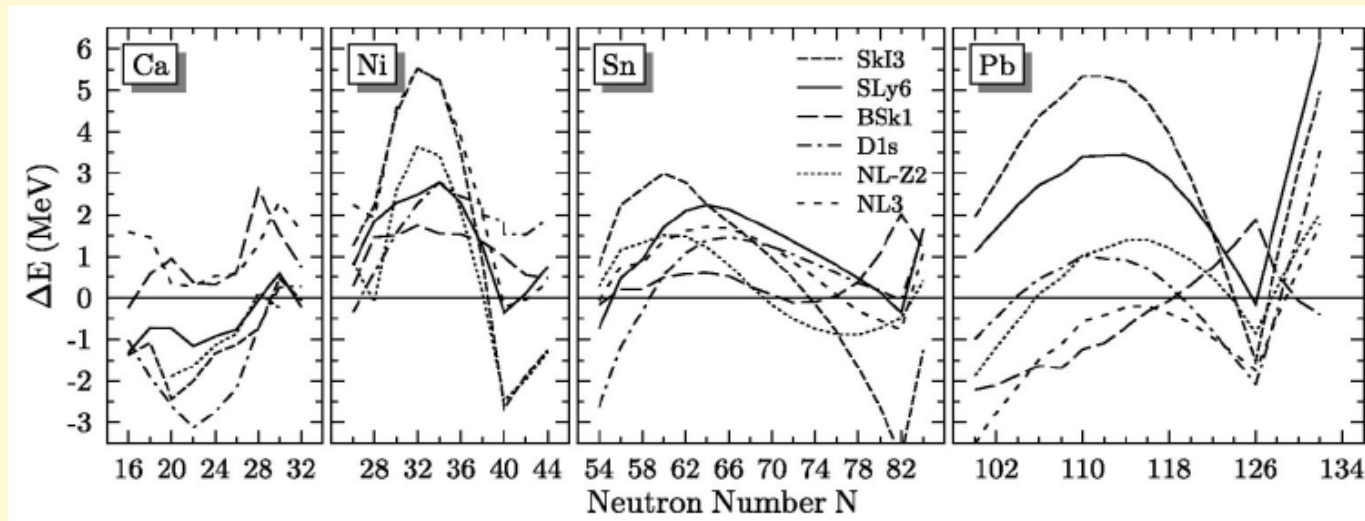
M. Bender, P. Heenen, and P.G. Reinhard,
Rev. Mod. Phys. 75, 122 (2003)

HF neutron single-particle energies, using several Skyrme forces, compared to experiment

M. Bender, P. Heenen, and P.G. Reinhard, Rev. Mod. Phys. 75, 122 (2003)



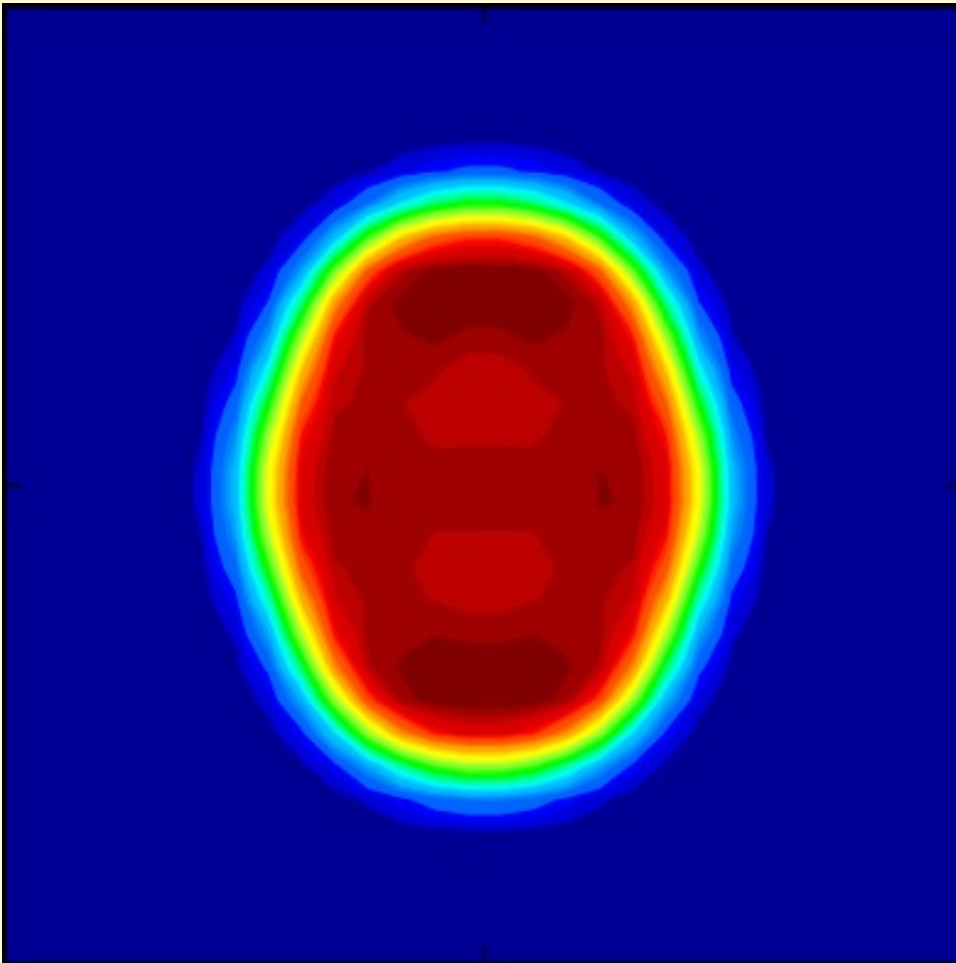
HF binding energies, calculated with different Skyrme forces. Plotted is energy difference between experiment and theory.



M. Bender, P. Heenen, and P.G. Reinhard,
Rev. Mod. Phys. 75, 122 (2003)

^{249}Bk : HF predicts positive quadrupole + hexadecapole deformation, in agreement with exp. data

6,300 static iterations, CPU time = 2h 50m (16 INTEL Xeon CPUs)



Convergence of total binding energy $\Delta E / E = 4.2 \times 10^{-10}$

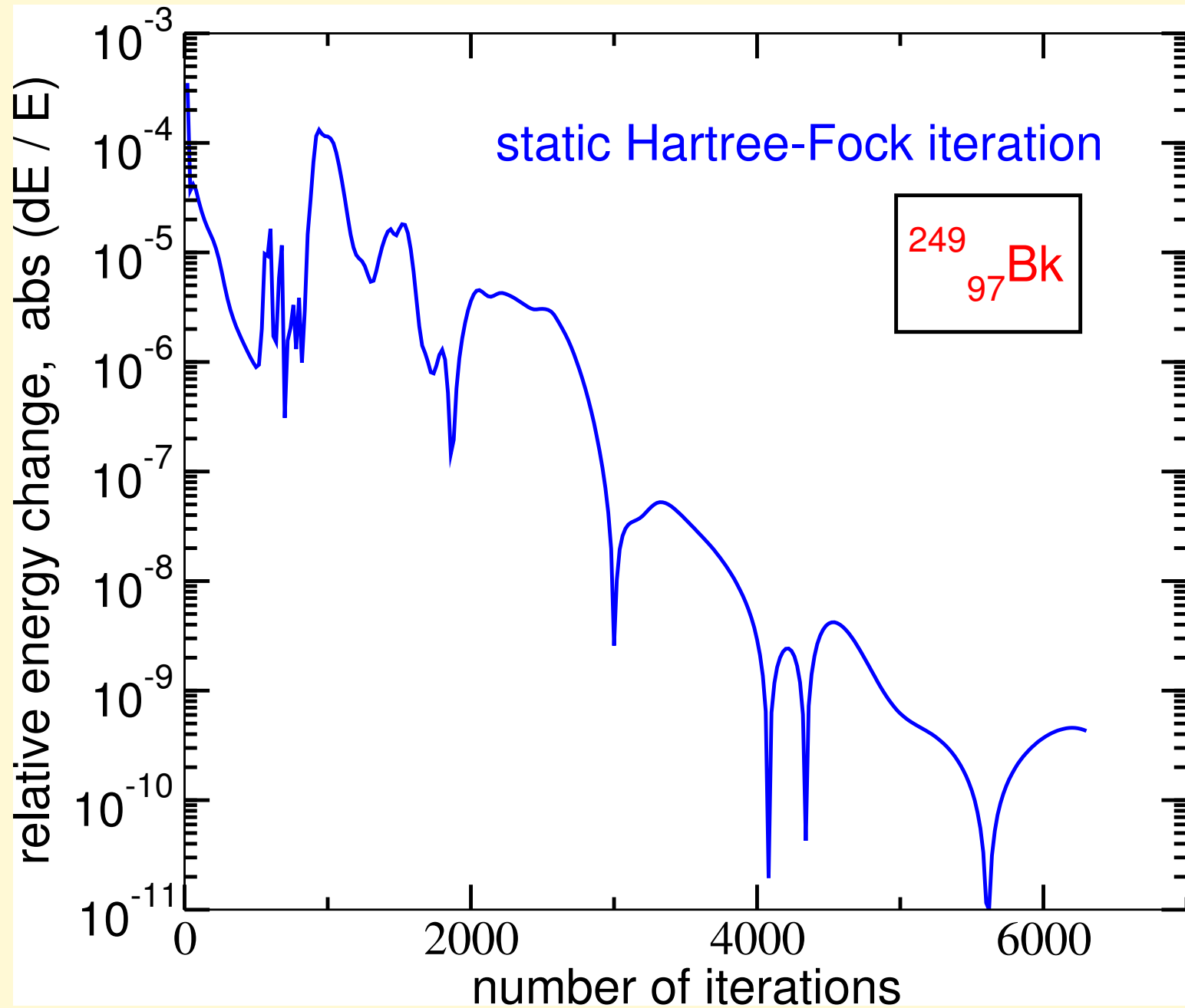
HF binding energy

= -1,875.11 MeV

exp. binding energy

= -1,864.02 MeV

accuracy = 0.6%



Constrained Hartree-Fock calculations: collective energy surface

Ref: Ring & Schuck, chapter 7.6

Add electric multipole operators Q_i to variational principle

$$\delta \left[\langle \Phi_0^{HF} | H | \Phi_0^{HF} \rangle - \sum_i \lambda_i \langle \Phi_0^{HF} | Q_i | \Phi_0^{HF} \rangle \right] = 0$$

↖ Lagrange multipliers

The values of Lagrange multipliers are determined from the **constraint** that the electric multipole operators have a given expectation value

$$\langle \Phi_0^{HF} | Q_i | \Phi_0^{HF} \rangle = q_i \longleftarrow \text{given}$$

As a result of constraints, one obtains the “collective energy surface”

$$E(q_i)$$

or more explicitly

$$E(q_{20}, q_{22}, q_{30}, q_{40}, \dots)$$

HF calculation with **quadrupole constraint**, for chain of **gadolinium** isotopes, using several Skyrme forces.

upper figure: collective **potential energy surface**

lower figure: ground state **deformation**, compared to exp. data

M. Bender, P. Heenen,
and P.G. Reinhard,
Rev. Mod. Phys. 75,
122 (2003)

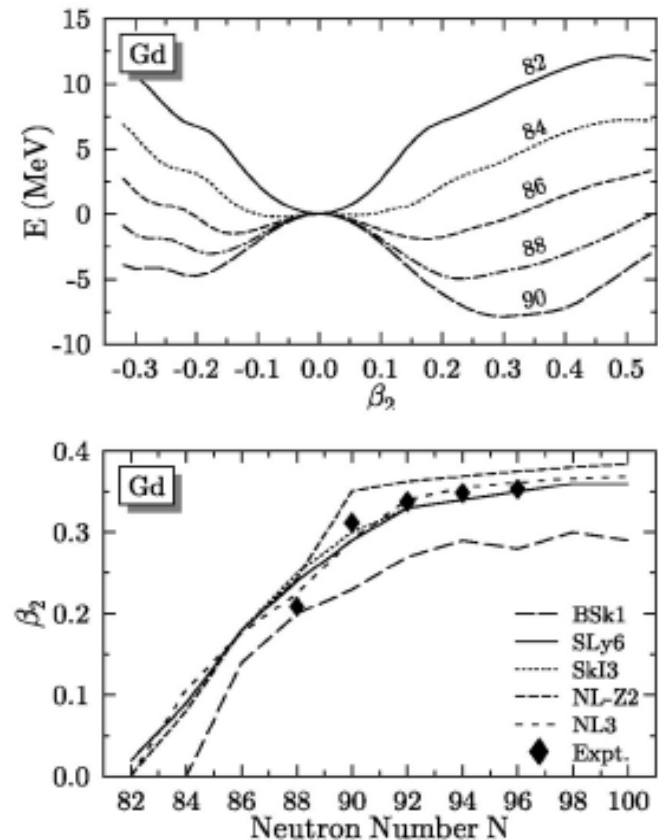


FIG. 13. Transition from spherical to deformed shapes in the chain of Gd isotopes. Upper panel: HF+BCS potential-energy surfaces calculated with the SLy6 interaction for neutron numbers ranging from 82 to 90. Lower panel: Ground-state deformation of Gd isotopes for several forces. Pairing is treated with the BCS method except for BSk1 for which the HFB method is used. Experimental values are taken from Raman *et al.* (2001).

3-D Skyrme HF calculation, with quadrupole constraint: double-humped fission barrier for ^{240}Pu

BÜRVENICH, BENDER, MARUHN, AND REINHARD

PHYSICAL REVIEW C **69**, 014307 (2004)

siderations to axially symmetric shapes. Our investigation also covers the prolate fission path only. It has to be kept in mind that novel fission paths may emerge for the heaviest of the nuclides discussed here, which start out from strongly oblate shapes and proceed through triaxial deformations [21]. For this and the reasons given above, our results provide an upper limit for the (static) fission barriers. This limitation holds also for most other work using self-consistent models published so far, as well as most of the results from mic-mac approaches.

The deformation energy curves are obtained with a constraint on the mass quadrupole moment $Q_{20}=\langle\hat{Q}_{20}\rangle$. For reflection-asymmetric shapes, we also fix the center of mass with a constraint on the mass dipole moment $\langle\hat{Q}_{10}\rangle=0$. The constraints are added to the energy functional by means of Lagrange multipliers [37]. Besides these constraints, the deformation energy is minimized with respect to all axial multipole moments $Q_{\ell 0}$ for protons and neutrons separately. In a

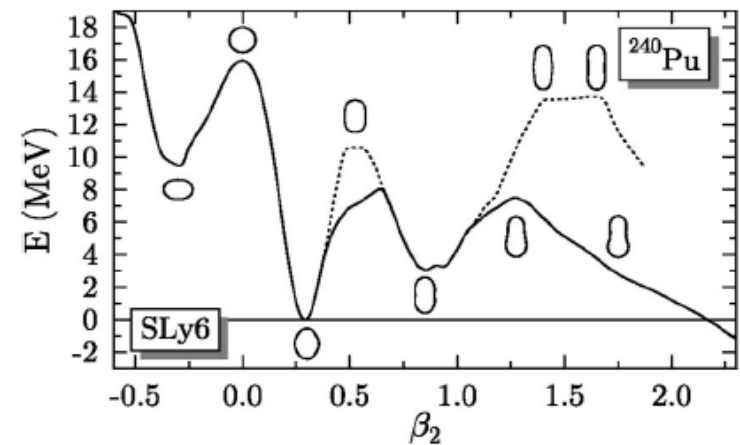


FIG. 1. Example for the double-humped fission barrier of the typical actinide nucleus ^{240}Pu . The dotted line denotes an axial and reflection-symmetric calculation, the full line denotes a triaxial (inner barrier) and axial and reflection-asymmetric calculation (outer barrier). The various shapes along the axial paths are indicated by the contours of the total density at $\rho_0=0.07\text{ fm}^{-3}$.

“Cranked” Hartree-Fock calculations: rotational bands

Ref: Ring & Schuck, chapter 7.7

Add total angular momentum operator to variational principle

$$\delta \left[\langle \Phi_0^{HF} | H | \Phi_0^{HF} \rangle - \omega(I) \langle \Phi_0^{HF} | J_x | \Phi_0^{HF} \rangle \right] = 0$$

↙ Lagrange multiplier = cranking frequency

The cranking frequency $\omega(I)$ depends on ang. mom. quantum number I ; its value is determined from the constraint condition

$$\langle \Phi_0^{HF}(\omega(I)) | J_x | \Phi_0^{HF}(\omega(I)) \rangle = \sqrt{I(I+1)}$$

As a result of this constraint, one obtains “rotational bands” $E(I)$

which agree much better with experiment than simple collective models (microscopic moments of inertia change as function of ang. momentum!)

Cranked HF calculation in 3-D, for two Skyrme forces

Ref: M. Yamagami and K. Matsuyanagi, Nucl. Phys. A672 (2000) 123

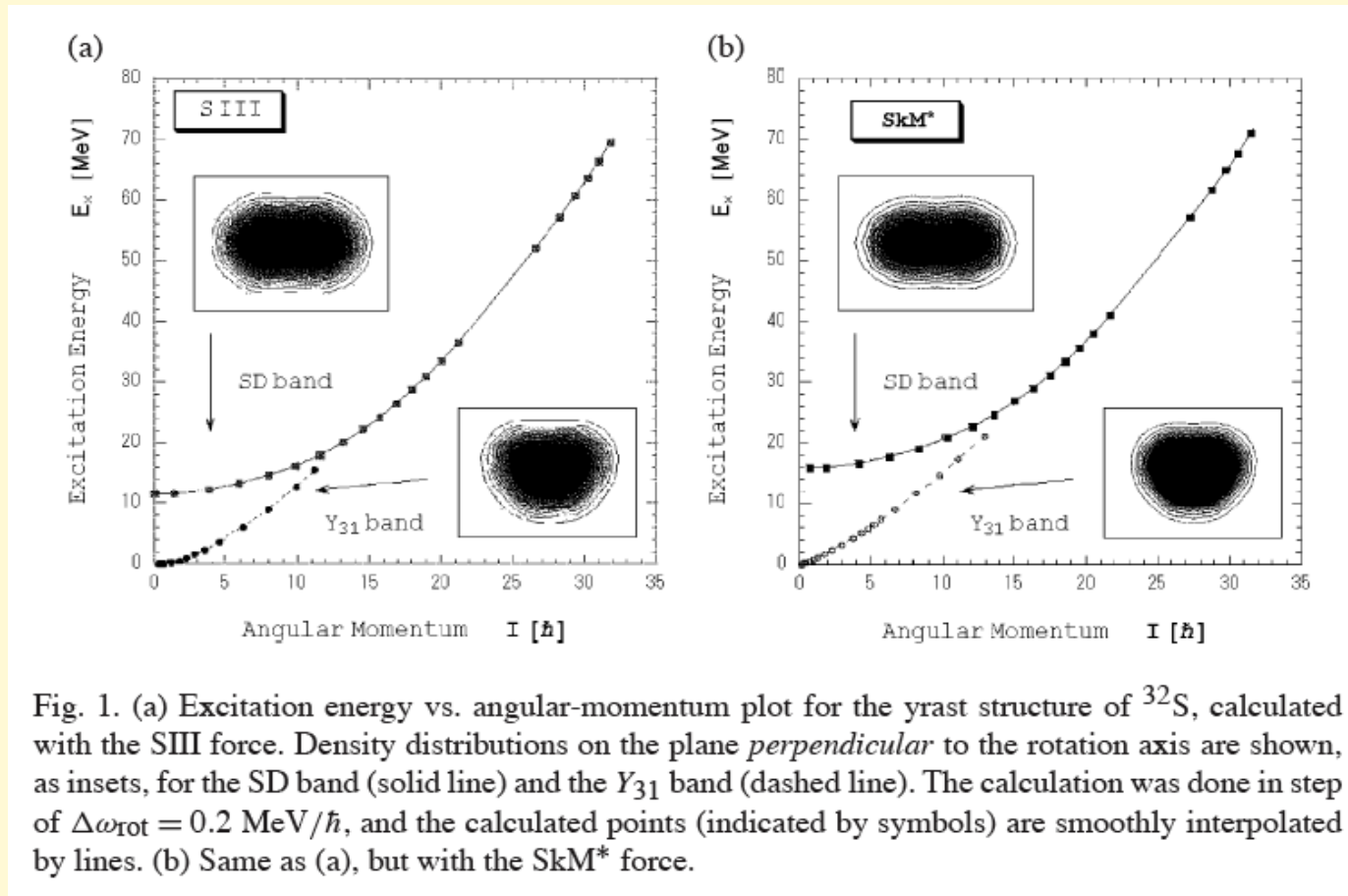


Fig. 1. (a) Excitation energy vs. angular-momentum plot for the yrast structure of ^{32}S , calculated with the SIII force. Density distributions on the plane *perpendicular* to the rotation axis are shown, as insets, for the SD band (solid line) and the Y_{31} band (dashed line). The calculation was done in step of $\Delta\omega_{\text{rot}} = 0.2 \text{ MeV}/\hbar$, and the calculated points (indicated by symbols) are smoothly interpolated by lines. (b) Same as (a), but with the SkM* force.

Cranked HF calculation in 3-D, for two Skyrme forces

Ref: M. Yamagami and K. Matsuyanagi, Nucl. Phys. A672 (2000) 123

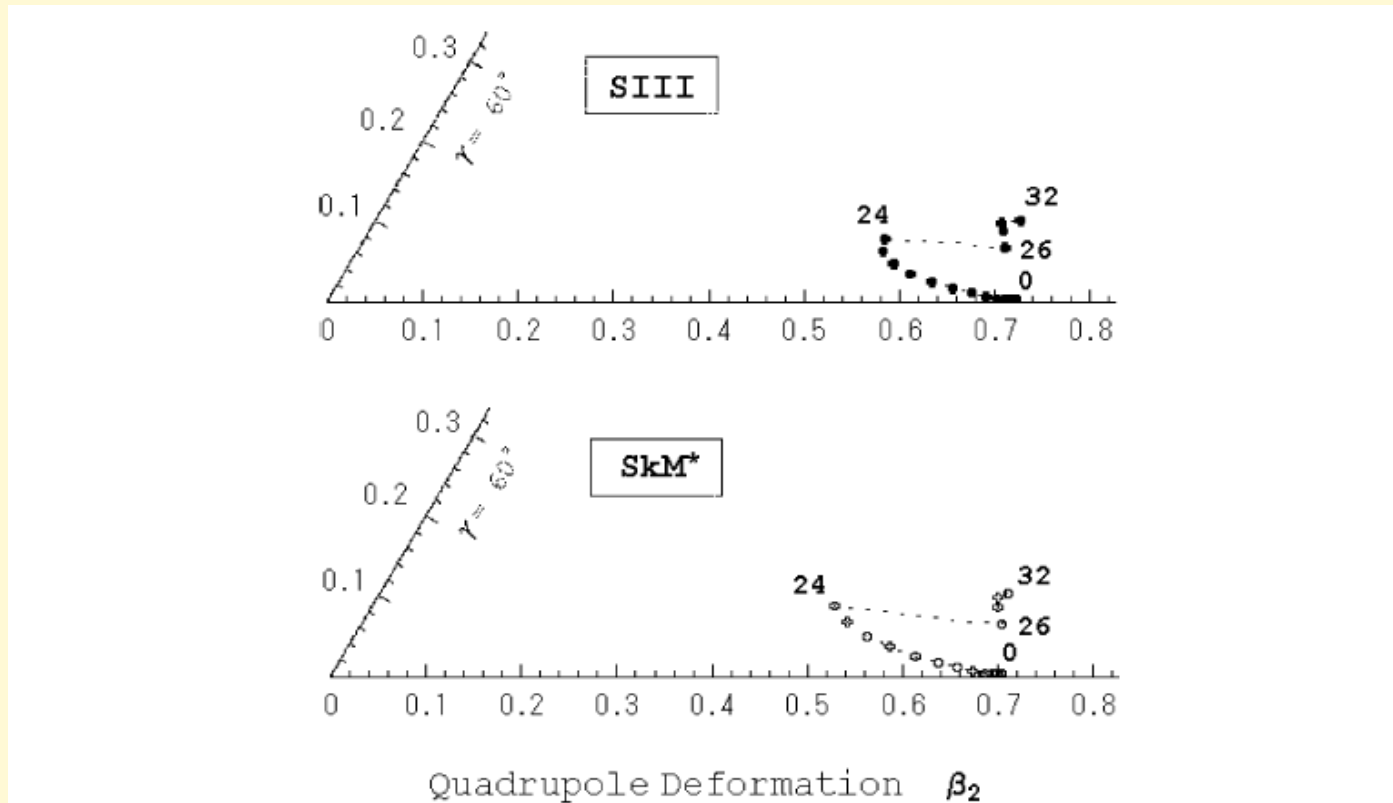


Fig. 6. Shape evolution as a function of angular momentum, plotted in the (β_2, γ) plane for the SD and HD-like configurations in ^{32}S . Results calculated with the SIII and SkM* forces are shown separately.